Electronic origin of ferroelectricity in multiferroic math xmlns="http://www.w3.org/1998/Math/MathML">mrow>msub>mi>Lu/mi>mrow>mn>0.5/mn>/mrow>/msub>msub>mi>Sc/mi>mrow>mn>0.5/mn>/mrow>/msub>msub>mi>FeO/mi>mn>3/mn>/msub>/mrow>/math>

Jeong Kyu Kim, Bongjae Kim, Dong-Hwan Kim, Kyoo Kim, Arata Tanaka, Younghak Kim, Sang-Wook Cheong, Kyung-Tae Ko, and Jae-Hoon Park

Phys. Rev. B **108**, 155152 — Published 31 October 2023

DOI: 10.1103/PhysRevB.108.155152

Electronic origin of ferroelectricity in multiferroic $Lu_{0.5}Sc_{0.5}FeO_3$

Jeong Kyu Kim,[1,2] Bongjae Kim,[1,3] Dong-Hwan Kim,[1,2,4] Kyoo Kim,[5] Arata Tanaka,[6] Young-Hak Kim,[7] Sang-Wook Cheong,[8,9] Kyung-Tae Ko,[1,2,10,*] and Jae-Hoon Park[1,2,*]

[1] *Max Plank Korea/POSTECH Center for Complex Phase Materials, Pohang 37673, Korea*
[2] *Department of Physics, Pohang University of Science and Technology, Pohang 37673, Korea*
[3] *Department of Physics, Kunsan National University, Gunsan 54150, Korea*
[4] *Samsung Electronics Co, Ltd, 1 Samsungjeonja-ro, Hwasung-si, Gyeonggi-do 445-701, South Korea*
[5] *Korea Atomic Energy Research Institute, Daejeon 34057, Korea*
[6] *Department of Quantum Matter, ADSM Hiroshima University, Higashi-Hiroshima 739-8530, Japan*
[7] *Pohang Accelerator Laboratory, POSTECH, Pohang 37673, Republic of Korea*
[8] *Rutgers Center for Emergent Materials & Department of Physics and Astronomy, Rutgers University, Piscataway, New Jersey 08854, USA*
[9] *Lab of Pohang Emergent Materials, POSTECH, Pohang 37673, Korea*
[10] *Korea Basic Science Institute, Daejeon 34133, Korea*

(Dated: August 30, 2023)

We conducted a comprehensive study on the electronic structure of a multiferroic $Lu_{0.5}Sc_{0.5}FeO_3$ single crystal using a range of techniques, including X-ray absorption spectroscopy, cluster model calculations, and *ab initio* analyses. Our X-ray linear dichroism measurements revealed strong hybridization of A-site d orbitals with neighboring O p orbitals. The hybridization strength of Lu $5d$ turns out to be not only much stronger but also more anisotropic than that of Sc $3d$, leading to a huge ligand-field splitting between the out-of-plane a_{1g} orbital state and in-plane e_g^π one. Based on our findings, we confirmed that Lu has a significantly larger ferroelectric energy gain compared to Sc. By combining our results with a simple phononic potential energy, we were able to quantify the ferroelectric energy landscape, which agrees well with the *ab initio* calculation result. Through a comparative analysis of Lu $5d$ and Sc $3d$ cases, we revalidate the rehybridization mechanism as the origin of ferroelectricity appearing in h-A(Mn,Fe)O_3 family.

I. INTRODUCTION

Multiferroic compounds have been intensively investigated for the last two decades because they offer extensive opportunities to study couplings of charge, spin, orbital, and lattice. Furthermore, these compounds hold promise for the development of future magneto-electric devices[1–5]. In these compounds, multiple ferroic orders coexist and the order parameters interact with each other[6–9]. In most multiferroics classified as type-II, ferroelectricity is induced by inverse magneto-electric coupling, resulting in a relatively smaller magnitude of ferroelectric polarization ($P_{\rm E}$) compared to that in typical ferroelectric materials.

Hexagonal manganites and ferrites, h-A(Mn,Fe)O_3, belong to the distinguished family classified as a type-I multiferroics since $P_{\rm E}$, which reaches 4 - 9 μC/cm^2[10–13] as large as that of the famous ferroelectric material $BaTiO_3$[14], is attributed to off-centered non-magnetic A-site ions. Due to the significantly small ionic size of A-sites, the system is stabilized in a layered hexagonal structure with the corner shared network of bipyramidal (Mn,Fe)O_5 cages as shown in Fig. 1(a). In (Mn,Fe)O_5 polyhedra, B-site magnetic ions are surrounded by two apical ($O_{\rm A}$) and three planar ($O_{\rm P}$) oxygen ions. Ferroelectricity stems from structural distortions that involve a phonon softening of K_3-mode as described in Fig. 1(b,c)[15–17]. Here, A-site ions shift to be off-centered, and A$-O_{\rm P}$ bonding lengths become strongly asymmetric along the c-axis, while B-site ions sit on the c-inversion center despite of cooperative buckling of (Mn,Fe)O_5 cages, resulting in a 1:2 ferri-type ferroelectric structure[18].

The ferroelectricity of $YMnO_3$ has been discussed about geometrical frustration and rehybridization mechanism. According to the former perspective, the displacement of Y ions primarily results from the in-and-out buckling of MnO_5 cages, with minimal influence from rehybridization[19]. In contrast, the latter perspective suggests that ferroelectricity arises from the rehybridization mechanism of d^0-ness Y ion, specifically due to the anisotropic bonding between Y and $O_{\rm P}$ ions[20]. Intense investigations have been followed on related systems. The magnetoelectric coupling has garnered significant interest[8,21,22]. Notably, h-AFeO$_3$ systems have drawn attention due to the presence of Fe^{3+} ions, which exhibit a larger local moment, resulting in a higher antiferromagnetic T_N compared to Mn^{3+} without orbital degrees of freedom[11,23]. However, stabilizing h-AFeO$_3$ single crystal is challenging due to the small ionic size of Fe^{3+}, leading to a reduced tolerance factor; thus, the bulk crystalline form has not been rigorously studied[11,24,25]. Although ferroelectricity and magnetic properties of h-AFeO$_3$ have been studied intensively, the detailed electronic structure of the single crystalline sample has been barely explored.

Recently, it has been reported that Sc substitution in $LuFeO_3$ can stabilize the hexagonal form near $Lu_{0.5}Sc_{0.5}FeO_3$ (LSFO) composition[21,24,26–28]. Its ferroelectric transition temperature is $T_{FE} \sim 1010$ K with

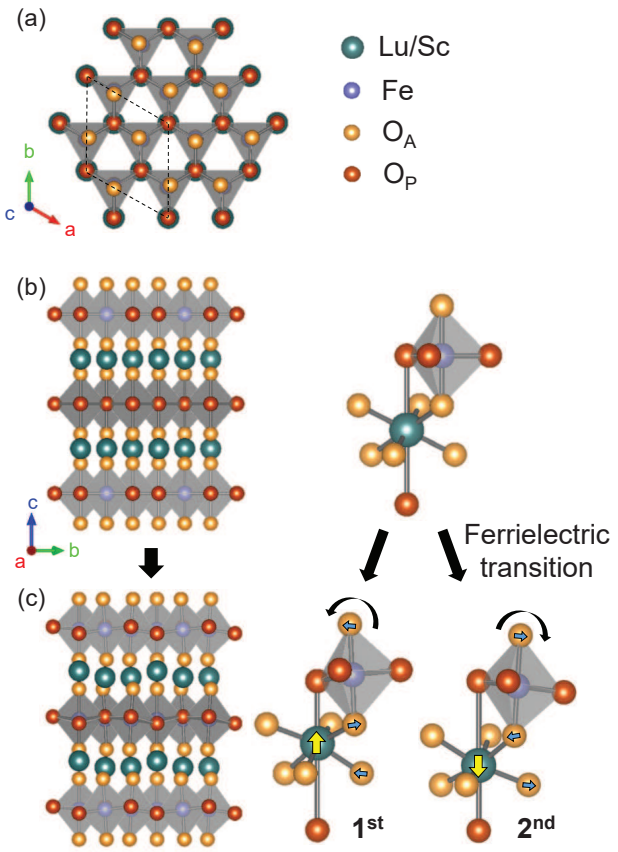

FIG. 1. (a) The structure of $Lu_{0.5}Sc_{0.5}FeO_3$ consists of bipyramidal FeO_5 cages that share O_P ions, forming a triangular layered structure. (b)(c) During the ferroelectric transition, A-site ions move up and down with a 1:2 ratio from the centrosymmetric position, causing FeO_5 cages to tilt by the longer and shorter bonds.

the clear hysteresis loop of electric polarization ($P_E \sim 4\mu C/cm^2$ at low temperature)[21,29]. Non-collinear spin magnetic order was observed below $T_N = 172$ K, and spin reorientation transition occurs at $T_R = 45$ K[21]. In addition, a magnetic anomaly was reported in a polycrystalline sample at $T_A = 445$ K although the magnetic state in $T_N < T < T_A$ is still unresolved[29]. An intriguing point is that LSFO has the mixture of two different A-site atomic configurations - $Sc^{3+}(3d^0)$ and $Lu^{3+}(4f^{14}5d^0)$. The effects of hybridization strengths and ionic sizes are expected to have a significant impact on the ferroelectric properties. Hence, conducting electronic investigations on LSFO can help reveal the role of rehybridization in the h-A(Mn,Fe)O_3 family, as well as provide clues to explain the stabilization of ferroelectric LSFO.

In this paper, we investigated the electronic structure and ferroelectric nature of LSFO through comprehensive spectroscopic and theoretical studies. Using polarization-dependent X-ray absorption spectroscopy (XAS), we explored the detailed electronic structure of LSFO, specifically examining the hybridization effects of Lu, Sc, and Fe cations. To extract precise electronic parameters, we conducted cluster model calculations that incorporated full Coulomb multiplets and configuration interactions (CI). These calculations allowed us to analyze linear dichroism (LD) spectra at Sc and Fe L-edges, as well as O K-edge. Our findings demonstrate a notable disparity in hybridization strength between A-site Lu and Sc ions, leading to a distinct shift in the energy level position of a_{1g} state due to the anisotropic bonding. Consequently, the reduction of total energy resulting from ferroelectric distortions is much more pronounced for Lu compared to Sc, primarily due to its larger and anisotropic hybridization strength. By incorporating a moderate phononic potential energy, we successfully characterized the ferroelectric energy landscapes, which exhibited quantitative agreement with those obtained from *ab initio* calculation analyses. Finally, we emphasize the importance of A-site hybridization in comprehending the ferroelectric distortions in h-A(Mn,Fe)O_3.

II. METHODS

High-quality LSFO single crystals were grown using a high-pressure floating zone method[21], and we obtained clean plate-shaped crystals with antiferro/weak-ferromagnetism[29]. XAS measurements were carried out at beamline 2A in Pohang Light Source. XAS spectra were acquired in total electron yield (TEY), where drain currents from the sample and a reference gold mesh were simultaneously recorded to normalize the raw TEY spectrum with beam intensity. The measurements were performed at $T \sim 250$ K under non-magnetic conditions and a clean surface of the sample was obtained through cleaving under ultra-high vacuum $\sim 1 \times 10^{-10}$ Torr. LD spectra were measured at Fe and Sc $L_{3,2}$-edges and O K-edge. The LSFO single crystal was mounted on a copper sample holder, with the normal axis aligned with the crystal c-axis. The beam incidence vector was fixed at 70° to the normal axis and two linear polarizations of $\sigma-$pol. and $\pi-$pol. were switched in the elliptically polarized undulator to obtain $E \parallel c$ and $E \perp c$ spectra, respectively.

We utilized XTLS 9.0, a full multiplets CI calculation code[30], to reproduce and analyze measured spectra. In CI model calculations, we incorporated the realistic parameters of crystal field (H_{CF}) and hybridization (H_{HY}) in distorted local structures from D_{3h} for FeO_5 and from D_{3d} for (Lu,Sc)O_8[31]. Those parameters are essential to consider the effects of anisotropic bonding in off-centered (Lu,Sc)O_8 sites. We analyzed O K-edge spectra using identical parameters and took into account separate oxygen sites to account for different bond lengths. We included up to second charge transfer states, $d^n \oplus d^{n+1}\underline{L} \oplus d^{n+2}\underline{L}^2$, and applied Harrison rule, $(pd\sigma) \propto d^{-7/2}$, to calculate the hybridization of different ligand oxygen ions.

First-principles calculations were performed using the plane-wave basis set and the projector-augmented-wave method implemented in the Vienna *ab initio* simulation

package.[32,33] Generalized gradient approximation (GGA) by Perdew, Burke, and Ernzerhof (PBE) exchange-correlation energy functional was used within the GGA $+U$ approach, with U=5 eV[34,35]. The plane-wave energy cutoff was set to 400 eV, and an $8 \times 8 \times 4$ k-point mesh was employed for a hexagonal unit cell containing 30 atoms. Various configurations of Lu and Sc sites were considered for LSFO, and full structural relaxation was performed until the Hellman-Feynman forces converged within 0.001 eV/Å. The most stable configuration exhibited a very similar volume compared to the experimental one, differing only by 0.14%[21,24], and this configuration was used for detailed analysis[36,37].

III. RESULTS AND DISCUSSION

Figure 2(a) and (b) show linear polarization-dependent X-ray absorption spectra (XAS) at Fe L-edge and Sc L-edge, along with the corresponding results from CI calculations. The red and blue colors represent spectra obtained using E $\parallel$ c and E $\perp$ c linearly polarized beams, respectively. Both spectra exhibit two white lines corresponding to $L_3(\underline{2p}_{3/2})$- and $L_2(\underline{2p}_{1/2})$-edge, which are attributed to the significant spin-orbit coupling of 2p core hole final states.

The white line for Fe L_3-edge is observed at the energy position of approximately 709 eV, indicating a typical Fe^{3+} oxidation state. The L_3-edge absorption and LD spectra exhibit three distinguishable states. The spectrum is mainly governed by the final state multiplets of $\underline{2p}3d^5_{\downarrow}3d^1_{\uparrow}$, leading to the primary reflection of ligand field split states in the spectrum. In FeO_5 bipyramidal cage, 3d orbitals are split into $e^{''}$ (d_{yz}, d_{zx}), $e^{'}$ (d_{xy}, $d_{x^2-y^2}$), and $a_1^{'}$ ($d_{3z^2-r^2}$) under D_{3h} symmetry. The sequential order of crystal field levels can be identified as e'', e', and a_1' by considering the absorption weight of the d orbitals and strong ligand field of two O_A ions on the $d_{3z^2-r^2}$ orbital.

Sc L-edge spectra in Figure 2(b) exhibit characteristic $\underline{2p}3d^1$ final state multiplets, with the four white lines corresponding to t_{2g} and e_g states at both L_3- and L_2-edges, showing minor anisotropy[38]. Given that ScO_8 cages are subject to D_{3d} symmetry, it is more appropriate to use e_g^{π}, a_{1g}, and e_g^{σ} notation, where the energy difference between e_g^{π} and a_{1g} levels is small. Notably, in Figure 2(b), the peak of E $\parallel$ c appears at higher energy than that of E $\perp$ c in the first and third peaks. This suggests that the energy position of a_{1g} level is higher than that of e_g^{π} level, indicating the strong hybridization with O_P ions, despite the compressive trigonal distortion caused by the six surrounding O_A ions with shorter bonding lengths.

The detailed electronic structure was examined using CI model calculations. Parameters were optimized within a reasonable range, including ionic positions under the same local symmetry. The reproduced spectra, shown in Fig.2, closely match the experimental spectra for both Fe and Sc L-edges, including the position and intensity of the multiplet structure. This indicates that the calculated electronic structure excellently explains the system, despite slight differences in parameters. Furthermore, we re-examined the electronic structure by reproducing Oxygen K-edge. A detailed explanation of parameters and structure will be provided in the discussion of O K-edge.

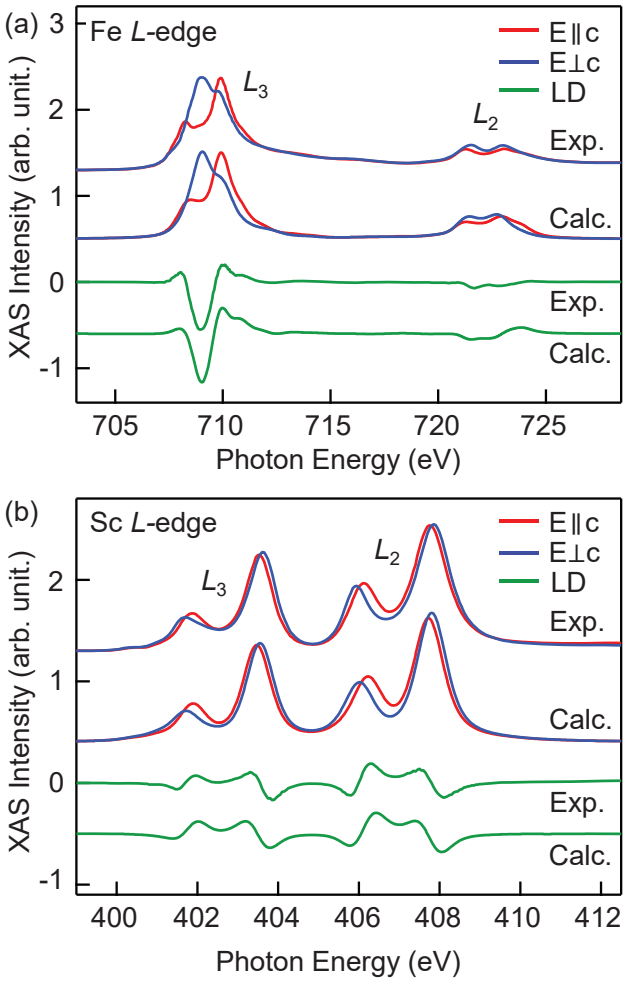

FIG. 2. XAS, LD, and CI calculation spectra of the (a) Fe and (b) Sc L-edges. Red(Blue) lines represent E $\parallel$ c (E $\perp$ c) spectra and green lines correspond to LD spectra (E $\parallel$ $c-$E $\perp$ c).

O K-edge XAS spectra and results of CI calculation are displayed in Fig.3. The first principle calculation is added to verify the results. The spectra measured using E $\parallel$ c and E $\perp$ c linearly polarized beams are indicated by red and blue colors, respectively. The spectra reflect the presence of oxygen 2p holes in unoccupied conduction bands, specifically anti-bonding states, due to hybridization. The full range spectra are displayed in the inset. The first region from 528 to 532 eV corresponds to Fe $3d$ hybridized state, where the $e^{''}$, $e^{'}$, and $a_1^{'}$ states are identified in the order. The detailed features of spectra are successfully reproduced in the CI model calculation, as shown in Fig.3(a), using the same parameters in Fe

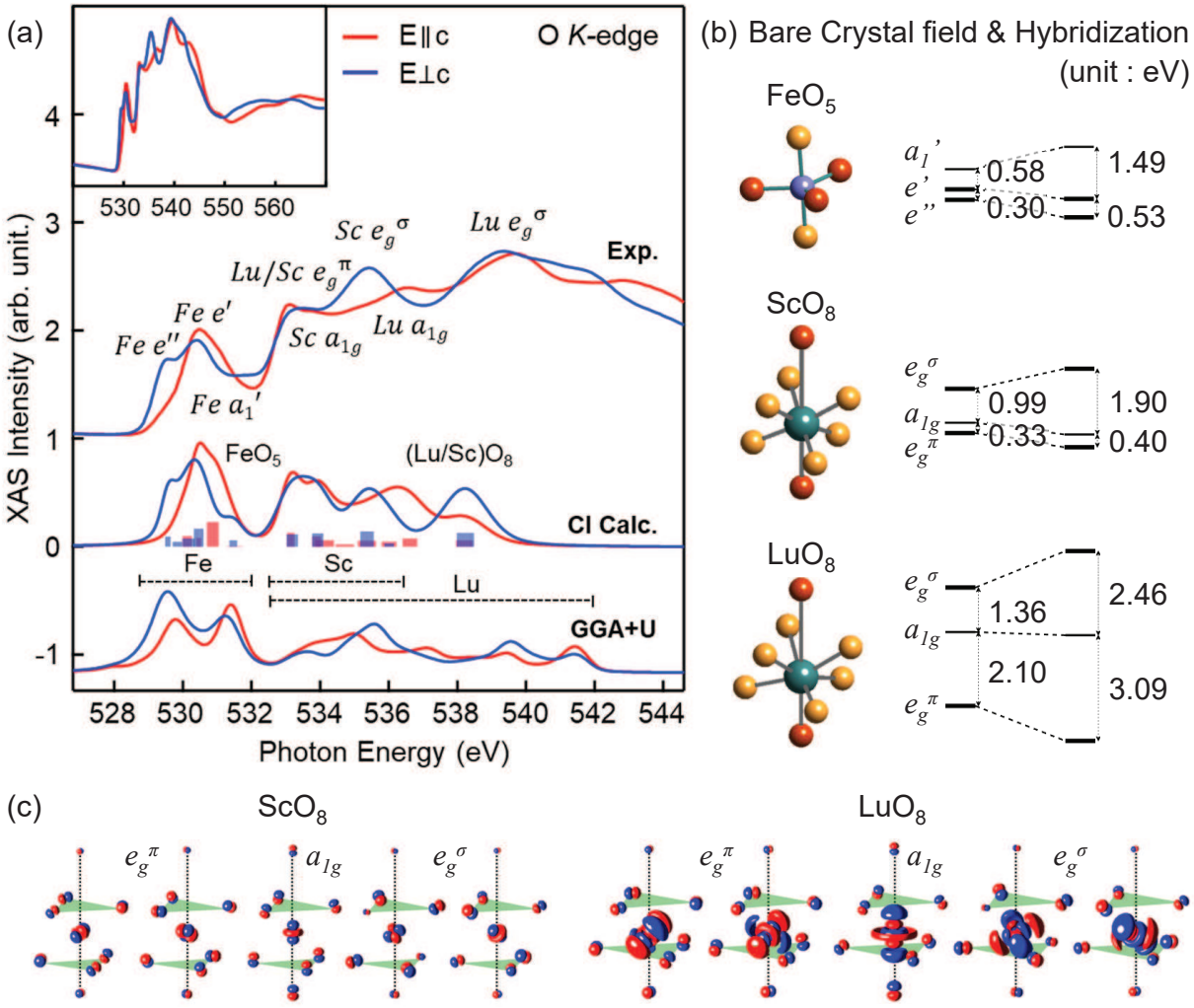

FIG. 3. (a) XAS spectra of O K-edge are displayed with CI and *ab initio* calculation results. Red(Blue) lines indicate E ∥ c (E ⊥ c) spectra. The energy level states and hybridized cations are labeled in the figure. (b) Local structures and energy level splittings of Fe, Sc, and Lu sites are shown. Here, we added up the spectra of upward and downward sites for Lu(Sc) with a 1:2 ratio to mimic the ferroelectric structure. The bare CF splitting and final splitting including hybridization were obtained by CI calculation. (c) The related orbitals are displayed with 3d and 5d states. These anti-bonding states considering the crystal field and hybridization effect are drawn with hydrogenic orbitals. e_g^π and e_g^σ orbitals hybridize mostly with six O_A ions while a_{1g} orbital significantly hybridizes with nearby O_P.

L-edge calculation. The energy difference (∼ 0.6 eV) between 2p hole final states in O_A and O_P was considered[20].

O 2p states hybridized with Sc 3d and Lu 5d are located above 532 eV. While the measured spectra are similar to those of $LuFeO_3$ and $YbFeO_3$[39], E ⊥ c polarized peak is observed around 535 eV. In this structure, A-site ion is surrounded by six O_A and two O_P ions, and D_{3d} symmetry splits d-orbitals into e_g^π, a_{1g} and e_g^σ states. As shown in Fig. 3(c), the hybridized O 2p ligands of e_g^σ states mainly consist of p_x and p_y orbitals, as the six nearby oxygen atoms exhibit a compressive trigonal distortion. Therefore, the newly induced E ⊥ c peak is attributed to the ligand hole state of Sc e_g^σ. The total splitting of Sc sites is ∼ 2.2 eV, while that of Lu sites is ∼ 6.2 eV, as shown in Fig.3(a). We examined the relative hybridization strengths of Sc and Lu sites in the CI calculations and found that the calculated spectra match the measured ones well.

Fig.3(b) displays the detailed energy level splittings. Initially, we applied a bare crystal field potential with $\Delta E(e' - e'') = 0.30$ eV and $\Delta E(a_1' - e') = 0.58$ eV, resulting in a final ligand field splitting of 0.53 eV and 1.49 eV for Fe cluster[40]. These energy splittings exhibit slight differences from previous studies[41,42], which we attribute to the varying sizes of A-site ions and the resulting local structures between LSFO and $LuFeO_3$ thin films. These differences are important in describing the inter-site superexchange interaction and the resulting noncollinear AFM order[43,44]. It is worth noting that the electronic structure of Fe could provide a

TABLE I. The hybridization strength of each bonding state in the cluster is tabulated. Units are expressed in electron volts (eV).

	Sc^1O_8	Sc^2O_8	Lu^1O_8	Lu^2O_8
e_g^σ	3.88	3.86	8.90	9.09
a_{1g}	2.53	2.48	7.20	7.44
e_g^π	2.33	2.31	5.37	5.49

pathway to create weak ferromagnetism in $h-A\mathrm{FeO_3}$[8], as $\mathrm{FeO_5}$ bipyramidal symmetry possesses degenerate $e^{'}$ and $e^{''}$ orbitals, which are a source of single ion anisotropy[45]. Therefore, charge transfer to the minority spin orbital[42] or deliberate hole doping to implement Fe^{2+} can enhance weak ferromagnetism[13,24,42,46] and enable magneto-electric coupling[8].

The energy level splittings of $\Delta E(a_{1g}-e_g^\pi)=0.33$, 2.10 eV and $\Delta E(e_g^\sigma-a_{1g})=0.99$, 1.36 eV are obtained through a bare crystal potential for Lu and Sc, respectively. By including hybridization, these splitting become $\Delta E(a_{1g}-e_g^\pi)=0.40$, 3.09 eV and $\Delta E(e_g^\sigma-a_{1g})=1.90$, 2.46 eV as final ligand field splittings. These are averaged results obtained by separately calculating the spectrum for upward and downward sites. The large difference in the crystal field and hybridization strength between the two ions is natural, as the radial function of Lu's $5d$ orbitals is more extended than that of Sc's $3d$ orbitals, resulting in more than twice the total splitting that accompanies the hybridization in $(\mathrm{Lu,Sc})O_8$ cage[47]. The hybridization strengths used in the calculations are tabulated in Table.I. As a result of the difference in hybridization, Lu hybridized states exhibit significantly larger peaks over a wide energy range, while only e_g^σ level of Sc's hybridized state shows a marked peak. To gain a better understanding of the bonding states, Fig.3(c) visualizes the anti-bonding states obtained through a simple matrix calculation, taking into account both the crystal field and hybridization effects. The size of the ligand orbitals is proportional to the ratio of the states. This visualization helps estimate the participation of orbitals in the bonding states.

One of the interesting points is the difference in the anisotropic hybridization of Lu and Sc. From the absorption spectra, we can observe that the energy splitting between e_g^π and a_{1g} levels of Sc is not as large as that of Lu and its polarization dependence is not as prominent as Lu's. Since ferroelectric displacement is responsible for anisotropy and larger e_g^π-a_{1g} splitting, we have to apply a more distorted structure to Lu. This assumption is contrary to a general expectation that a small ion can move easily, but it supports the idea of a large hybridization strength of the Lu ion. The energy gain through hybridization with Lu is significant enough to overcome the elastic energy cost, leading to more distortion in Lu to avoid overlap with the apical oxygen, while Sc remains

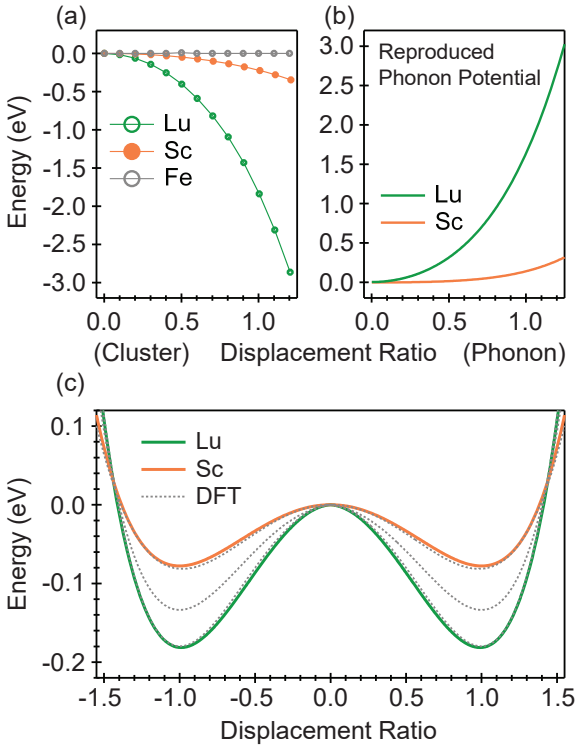

FIG. 4. (a) Cluster calculations reveal significant energy gain resulting from the displacement of Lu and Sc. (b) Phononic potential energy was reproduced to achieve the best fit for *ab initio* calculations. (c) Total energy landscapes obtained by adding (a) and (b) for $\mathrm{LuFeO_3}$ (orange) $\mathrm{ScFeO_3}$ (green) compared with corresponding *ab initio* calculation results. Additionally, the *ab initio* calculation result for $\mathrm{Lu_{0.5}Sc_{0.5}FeO_3}$ is presented in the figure.

less distorted[48]. This result is in agreement with reference 47 (Fig.4) in that Lu rich condition induces shorter Lu/Sc-O bonding length and larger θ angle in narrow doping region[49].

To supplement the results, we performed *ab initio* calculations. The calculated PDOS is displayed at the bottom of Fig.3 (a). Despite the fundamental difference in calculations, overall features match satisfactorily including ranges, positions, and polarizations. One of the notable differences is the PDOS area of Lu and Sc hybridized region. When fixing the area of Fe hybridized region, the area of Lu(Sc) hybridized region in *ab initio* calculation underestimates about 40 % compared to the CI calculation. This seems to be a fundamental limitation in describing d^0 system under the one-electron approximation where many-body effects are partially included by parameter U.

We compared a ferroelectric energy landscape obtained from the cluster and *ab initio* calculations. While cluster calculations accurately capture many-body and bonding effects based on the local structure, they do not consider elastic phonon effects. To make a fair comparison, we constructed an artificial phononic potential energy that incorporates modest fourth and sixth-order terms,

considering the large displacement of ferroelectric distortions, in addition to the second-order harmonic term[17,50]. Fig.4 panel (a) displays the total energy reduction obtained from the cluster calculation, (b) shows the constructed phononic potential energy, and (c) presents the total energy obtained by adding (a) and (b), in comparison to *ab initio* calculation results based on the ferroelectric distortion ratio. Notably, the cluster calculation successfully reproduced the ferroelectric double-well potential using a simple phononic potential energy, in agreement with the *ab initio* results.

One can observe energy reduction by ferroelectric distortion is much larger for Lu (∼1.8 eV) than Sc (∼0.2 eV). As mentioned earlier, this implies that the large 5d orbital, which exhibits strong hybridization, contributes to a substantial energy reduction in combination with the d^0 configuration. Additionally, the phononic potential energy for Lu is also much larger than that for Sc. This is attributed to the larger radius of Lu and its highly distorted position resulting from strong anisotropic bonding. This finding not only provides the detailed electronic structure of 5d and 3d orbitals in Lu and Sc but also verifies d^0-ness rehybridization mechanism itself. Besides, it is expected that this mechanism is generally applicable to h-R(Mn,Fe)O_3 system that shares the same d^0 configuration.

IV. SUMMARY AND CONCLUSION

In summary, we investigated the electronic structure of $Lu_{0.5}Sc_{0.5}FeO_3$. The measured LD spectra are well reproduced in CI calculation, and Sc and Lu's ions exhibit a huge difference in hybridization strength, more than twice in Lu. Lu ion shows more anisotropic hybridization with O_P, and it results in wider energy separation between e_g^π and a_{1g} states. The ferroelectric energy gain obtained from the cluster calculations is significantly larger for Lu compared to Sc, due to the strong hybridization of Lu. The energy landscape constructed with a simple phononic potential energy describes the ferroelectric potential adequately. Our investigation recalls additional experimental and theoretical clarifications of the ferroelectric mechanism of h-R(Mn, Fe)O_3.

ACKNOWLEDGEMENT

This work was supported by the National Research Foundation of Korea(NRF) funded by the Ministry of Science and ICT(No. 2022M3H4A1A04074153 and 2020M3H4A2084417). B.K. also acknowledges support from NRF Grants No. 2021R1C1C1007017 and No.2021R1A4A1031920, and the KISTI Supercomputing Center (Project No. KSC-2022-CRE-0465). K.-T.K. was supported by the internal R&D program at KBSI (No. C330140). K.K. was supported by the internal R&D program at KAERI (524460-23). SWC was partially supported by the DOE under Grant No. DOE: DE-FG02-07ER46382.

* Corresponding author.
kkt0706@kbsi.re.kr
jhp@postech.ac.kr

[1] N. A. Spaldin, Science **309**, 391 (2005).
[2] S.-W. Cheong and M. Mostovoy, Nature Materials **6**, 13 (2007).
[3] D. Khomskii, Physics **2**, 20 (2009).
[4] S. Dong, J.-M. Liu, S.-W. Cheong, and Z. Ren, Advances in Physics **64**, 519 (2015).
[5] A. P. Pyatakov and A. K. Zvezdin, Physics-Uspekhi **55**, 557 (2012).
[6] M. Fiebig, T. Lottermoser, D. Fröhlich, A. V. Goltsev, and R. V. Pisarev, Nature **419**, 818 (2002).
[7] Y.-H. Chu, L. W. Martin, M. B. Holcomb, and R. Ramesh, Materials Today **10**, 16 (2007).
[8] H. Das, A. L. Wysocki, Y. Geng, W. Wu, and C. J. Fennie, Nature Communications **5**, 2998 (2014).
[9] H. Wang, Y. Zhang, K. Tachiyama, Z. Xia, J. Fang, Q. Li, G. Cheng, Y. Shi, J. Yu, T. Katayama, S. Yasui, and M. Itoh, Inorganic Chemistry **60**, 225 (2021).
[10] N. Fujimura, T. Ishida, T. Yoshimura, and T. Ito, Applied Physics Letters **69**, 1011 (1996).
[11] W. Wang, J. Zhao, W. Wang, Z. Gai, N. Balke, M. Chi, H. N. Lee, W. Tian, L. Zhu, X. Cheng, D. J. Keavney, J. Yi, T. Z. Ward, P. C. Snijders, H. M. Christen, W. Wu, J. Shen, and X. Xu, Phys. Rev. Lett. **110**, 237601 (2013).
[12] C. Xu, Y. Yang, S. Wang, W. Duan, B. Gu, and L. Bellaiche, Phys. Rev. B **89**, 205122 (2014).
[13] H. Yokota, T. Nozue, S. Nakamura, H. Hojo, M. Fukunaga, P.-E. Janolin, J.-M. Kiat, and A. Fuwa, Phys. Rev. B **92**, 054101 (2015).
[14] J. Shieh, J. H. Yeh, Y. C. Shu, and J. H. Yen, Materials Science and Engineering: B **161**, 50 (2009).
[15] C. J. Fennie and K. M. Rabe, Phys. Rev. B **72**, 100103 (2005).
[16] A. S. Gibbs, K. S. Knight, and P. Lightfoot, Phys. Rev. B **83**, 094111 (2011).
[17] D. Bansal, J. L. Niedziela, R. Sinclair, V. O. Garlea, D. L. Abernathy, S. Chi, Y. Ren, H. Zhou, and O. Delaire, Nature Communications **9**, 15 (2018).
[18] B. B. v. Aken, A. Meetsma, and T. T. M. Palstra, Acta Crystallographica Section C **57**, 230 (2001).
[19] B. B. van Aken, T. T. M. Palstra, A. Filippetti, and N. A. Spaldin, Nature Materials **3**, 164 (2004).
[20] D.-Y. Cho, J.-Y. Kim, B.-G. Park, K.-J. Rho, J.-H. Park, H.-J. Noh, B. J. Kim, S.-J. Oh, H.-M. Park, J.-S. Ahn, H. Ishibashi, S.-W. Cheong, J. H. Lee, P. Murugavel, T. W. Noh, A. Tanaka, and T. Jo,

Phys. Rev. Lett. **98**, 217601 (2007).
[21] S. M. Disseler, X. Luo, B. Gao, Y. S. Oh, R. Hu, Y. Wang, D. Quintana, A. Zhang, Q. Huang, J. Lau, R. Paul, J. W. Lynn, S.-W. Cheong, and W. Ratcliff, Phys. Rev. B **92**, 054435 (2015).
[22] S. Lee, A. Pirogov, M. Kang, K.-H. Jang, M. Yonemura, T. Kamiyama, S. W. Cheong, F. Gozzo, N. Shin, H. Kimura, Y. Noda, and J. G. Park, Nature **451**, 805 (2008).
[23] J. Liu, T. L. Sun, X. Q. Liu, H. Tian, T. T. Gao, and X. M. Chen, Advanced Functional Materials **28**, 1706062 (2018).
[24] A. Masuno, A. Ishimoto, C. Moriyoshi, N. Hayashi, H. Kawaji, Y. Kuroiwa, and H. Inoue, Inorganic Chemistry **52**, 11889 (2013).
[25] A. A. Bossak, I. E. Graboy, O. Y. Gorbenko, A. R. Kaul, M. S. Kartavtseva, V. L. Svetchnikov, and H. W. Zandbergen, Chemistry of Materials **16**, 1751 (2004).
[26] A. Masuno, A. Ishimoto, C. Moriyoshi, H. Kawaji, Y. Kuroiwa, and H. Inoue, Inorganic Chemistry **54**, 9432 (2015).
[27] J. Yang, C. Duan, J. R. D. Copley, C. M. Brown, and D. Louca, MRS Advances **1**, 565 (2016).
[28] J. White, K. Sinha, and X. Xu, Journal of Applied Physics **125**, 244101 (2019).
[29] L. Lin, H. M. Zhang, M. F. Liu, S. Shen, S. Zhou, D. Li, X. Wang, Z. B. Yan, Z. D. Zhang, J. Zhao, S. Dong, and J.-M. Liu, Phys. Rev. B **93**, 075146 (2016).
[30] A. Tanaka and T. Jo, Journal of the Physical Society of Japan **63**, 2788 (1994).
[31] D.-Y. Cho, S.-J. Oh, D. G. Kim, A. Tanaka, and J.-H. Park, Phys. Rev. B **79**, 035116 (2009).
[32] G. Kresse and J. Furthmüller, Physical Review B **54**, 11169 (1996).
[33] G. Kresse and D. Joubert, Physical Review B **59**, 1758 (1999).
[34] J. P. Perdew, K. Burke, and M. Ernzerhof, Physical Review Letters **77**, 3865 (1996).
[35] S. L. Dudarev, G. A. Botton, S. Y. Savrasov, C. J. Humphreys, and A. P. Sutton, Physical Review B **57**, 1505 (1998).
[36] R. D. King-Smith and D. Vanderbilt, Physical Review B **47**, 1651 (1993).
[37] R. Resta, Reviews of Modern Physics **66**, 899 (1994).
[38] F. M. F. de Groot, J. C. Fuggle, B. T. Thole, and G. A. Sawatzky, Physical Review B **41**, 928 (1990).
[39] S. Cao, K. Sinha, X. Zhang, X. Zhang, X. Wang, Y. Yin, A. T. N'Diaye, J. Wang, D. J. Keavney, T. R. Paudel, Y. Liu, X. Cheng, E. Y. Tsymbal, P. A. Dowben, and X. Xu, Phys. Rev. B **95**, 224428 (2017).
[40] For the CI calculation of Fe(Sc) L-edge, the fitting parameters are U_{dd} = 5(3) eV, U_{pd} = 6.5(4.5) eV, Δ = 4(4) eV, and Slator integrals for d-d and p-d Coulomb interactions are reduced by 80 % from the Hartree-Fock values obtained by using Cowan code. The $(pd\sigma) = -2.2(-2.4)$ eV and $(pd\pi) = 1.1(1.2)$ eV used for 2 Å bonding length, then relative hybridization strengths were derived using given structures and Harrison's rule.
[41] W. Wang, H. Wang, X. Xu, L. Zhu, L. He, E. Wills, X. Cheng, D. J. Keavney, J. Shen, X. Wu, and X. Xu, Applied Physics Letters **101**, 241907 (2012).
[42] S. Cao, X. Zhang, T. R. Paudel, K. Sinha, X. Wang, X. Jiang, W. Wang, S. Brutsche, J. Wang, P. J. Ryan, J.-W. Kim, X. Cheng, E. Y. Tsymbal, P. A. Dowben, and X. Xu, Journal of Physics: Condensed Matter **28**, 156001 (2016).
[43] E. C. Standard, T. Stanislavchuk, A. A. Sirenko, N. Lee, and S.-W. Cheong, Phys. Rev. B **85**, 144422 (2012).
[44] H. Wang, I. V. Solovyev, W. Wang, X. Wang, P. J. Ryan, D. J. Keavney, J.-W. Kim, T. Z. Ward, L. Zhu, J. Shen, X. M. Cheng, L. He, X. Xu, and X. Wu, Phys. Rev. B **90**, 014436 (2014).
[45] K.-T. Ko, H.-J. Noh, J.-Y. Kim, B.-G. Park, J.-H. Park, A. Tanaka, S. B. Kim, C. L. Zhang, and S.-W. Cheong, Phys. Rev. Lett. **103**, 207202 (2009).
[46] A. R. Akbashev, A. S. Semisalova, N. S. Perov, and A. R. Kaul, Applied Physics Letters **99**, 122502 (2011).
[47] L. Soriano, M. Abbate, J. C. Fuggle, M. A. Jiménez, J. M. Sanz, C. Mythen, and H. A. Padmore, Solid State Communications **87**, 699 (1993).
[48] Born effective charge obtained by evaluating the effective charge of CI model calculation is 6.14(5.15) for Lu(Sc) and 3.87 for Fe. From the BEC values, it can be inferred that the ferroelectric displacement is primarily induced by Lu and Sc, with Lu making a larger contribution compared to Sc.
[49] S. Deng, J. Li, D. R. Småbråten, S. Shen, W. Wang, J. Zhao, J. Tao, U. Aschauer, J. Chen, Y. Zhu, and J. Zhu, Nano Letters **21**, 6648 (2021).
[50] The coefficients for the second, fourth, and sixth order terms used to reproduce the phononic potential energy for Lu(Sc) are 1.13(0.045), 0.51(0.090), and 0.013(0.01), respectively. At the ferroelectric ground state, the phonon energy of Lu(Sc) is estimated to be 10(16) meV using a second-order approximation of the spring constant and atomic mass. This value is of the same order of magnitude as the few tens of meV obtained by inelastic neutron scattering in $YMnO_3$, which corresponds to a ferroelectrically induced optical phonon band(ref 49).